Proximity effect in planar superconducting tunnel junctions containing Nb/NiCu superconductor/ferromagnet bilayers

G. P. Pepe,[1] R. Latempa,[1] L. Parlato,[1] A. Ruotolo,[1] G. Ausanio,[1] G. Peluso,[1] A. Barone,[1] A. A. Golubov,[2] Ya. V. Fominov,[3] and M. Yu. Kupriyanov[4]

[1]*Coherentia INFM, Dipartimento Scienze Fisiche, Universitá di Napoli Federico II, Piazzale Tecchio n. 80, 80125 Napoli, Italy*

[2]*Faculty of Science and Technology, University of Twente, 7500 AE Enschede, The Netherlands*

[3]*L. D. Landau Institute for Theoretical Physics RAS, 119334 Moscow, Russia*

[4]*Nuclear Physics Institute, Moscow State University, 119899 Moscow, Russia*

(Received 9 June 2004; revised manuscript received 27 October 2005; published 14 February 2006)

We present experimental results concerning both the fabrication and characterization of superconducting tunnel junctions containing superconductor/ferromagnet (S/F) bilayers made by niobium (S) and a weak ferromagnetic $Ni_{0.50}Cu_{0.50}$ alloy. Josephson junctions have been characterized down to $T=1.4$ K in terms of current-voltage *I-V* characteristics and Josephson critical current versus magnetic field. By means of a numerical deconvolution of the *I-V* data the electronic density of states on both sides of the S/F bilayer has been evaluated at low temperatures. Results have been compared with theoretical predictions from a proximity model for S/F bilayers in the dirty limit in the framework of Usadel equations for the S and F layers, respectively. The main physical parameters characterizing the proximity effect in the Nb/NiCu bilayer, such as the coherence length and the exchange field energy of the F metal, and the S/F interface parameters have been also estimated.

DOI: 10.1103/PhysRevB.73.054506 PACS number(s): 74.50.+r, 85.25.−j

I. INTRODUCTION

The superconducting proximity effect in normal systems has been extensively investigated in the past.[1–4] Among experimental techniques tunneling spectroscopy measurements in normal/superconductor (N/S) systems reveal strong modifications of the electronic density of states (DOS) due to induced superconducting correlations in N. The electronic properties of the normal metal are modified within a distance of the order of the coherence length of the bulk superconductor, and the physical properties of the bilayer can be considerably different from those into the bulk.

Many theoretical and experimental studies have been proposed to study the spatially resolved DOS in a spatially inhomogeneous S/N structure.[5–9] Nowadays, many of the basic results from the proximity effect are widely used in device applications such as superconducting radiation detectors.[10]

The question of the proximity effect in the presence of a ferromagnetic layer, where an electronic spin splitting mechanism is present, still represents a research field of great interest.[11–19] In particular, the influence of an exchange field on the proximity density of states within a superconductor/ferromagnet (S/F) bilayer can have important implications both in fundamental physics, related to the coexistence of ferromagnetism and superconductivity, and in potential applications of S/F hybrid structures in the field of quantum computation.[20]

In the presence of an exchange field (E_{ex}) a specific superconducting state can be formed in the F layer, where the order parameter has an oscillatory spatial modulation. Moreover, the spatially oscillating order parameter contains nodes in which the phase changes by π.[21–30] Nontrivial behaviors of the critical temperature of S/F hybrid structures can be also a consequence of the aforementioned complex dependence of the order parameter on the exchange field.[18] Ryazanov *et al.*[31] have found a nonmonotonic temperature dependence of the critical current in SFS Josephson junctions with thin F layers and explained it by the crossover to a π state. It was further demonstrated[32] that this π state manifests itself in the half-period shift of the external magnetic field dependence of the transport critical current in triangular SFS arrays. An indirect proof of the π-phase shift has been proposed by Kontos *et al.*,[33] who studied the DOS in thin ferromagnetic films in contact with a superconductor. Afterward, other experimental evidence of Josephson π junctions has been published by other research groups.[34–37]

Tunneling spectroscopy was demonstrated to be a powerful tool for the investigation of many physical properties of proximized structures[6] such as S/F structures. For these systems the penetration of superconducting correlations in the F layer is strictly related to the exchange energy, and it is very short ranged (few nanometers for typical ferromagnetic *d* elements). The control of the interface quality over very short length scales represents still a challenge from an experimental point of view. As a consequence, lower exchange energies, achievable in ferromagnetic alloys, are needed in order to have length scales compatible with standard deposition techniques. Two types of alloys have been commonly and successfully employed: PdNi and NiCu, whose coherence lengths and Curie temperatures range between 2–25 nm and 10–200 K, respectively. So far, experiments with superconducting junctions and Josephson junctions have been performed. Recently, Kontos *et al.*[38] measured the DOS in Pd/Ni thin films with different Ni concentrations by tunneling spectroscopy in $Al/Al_2O_3/PdNi/Nb$ junctions. They explored both the paramagnetic and ferromagnetic regimes, and they extracted the electron-spin fluctuation coupling constant and the exchange field directly from tunneling

spectra. In the present paper, we report experimental results concerning both the fabrication and the characterization of Josephson tunnel junctions employing the well-established Nb-based technology and containing Nb/NiCu (S/F) bilayers as one of the two electrodes. The fabrication of high-quality Josephson tunnel junctions employing a S/F bilayer represents an important issue since Josephson tunnel structures offer the advantage of achieving potentially high-$I_C R_N$ products and a better control of junction's parameters. Moreover, Josephson tunnel junctions allow us to measure the quasi particle density of states with high energy and amplitude resolution, together with a direct knowledge of the current-phase relation between superconducting electrodes through the study of the Josephson current.

The superconductor is niobium (Nb) whereas the ferromagnet is the solid solution $Ni_{0.50}Cu_{0.50}$. In Sec. IIthe fabrication and characterization of the Josephson junctions are presented. The junctions were characterized in terms of *I-V* curves for temperatures down to $T=1.4$ K and of Josephson critical current as a function of the temperature and of an externally applied magnetic field. In Sec. IIIthe tunneling density of states on both sides of the S/F bilayer have been obtained by a numerical deconvolution of the *I-V* data recorded at low temperatures. Numerical DOS have been compared to theoretical predictions from a proximity model proposed for S/F bilayers in the dirty limit.[15] The difference between the clean and dirty limit lies in the presence of impurities or crystallographic dislocations in a dirty superconductor, which act as scattering centers for quasi particles. The comparison allowed us to estimate the main physical parameters characterizing the proximity effect in the investigated Nb/NiCu bilayer such as the coherence length ξ_F in the F layer, its exchange field energy E_{ex}, and the S/F interface properties.

II. EXPERIMENT

Thin films of a NiCu alloy were deposited by using a dc magnetron sputtering technique at a base pressure of 3×10^{-7} mTorr. The Corning Glass substrate was positioned at approximately 10 cm from the target, whose stochiometrical composition was $Ni_{0.5}Cu_{0.5}$. The Ar flux was fixed at 40 sccm during the deposition, while the sputtering power density and deposition rate were 10 W/cm^2 and 1.5 nm/s, respectively. The effective stoichiometry of the alloy in deposited films has been measured by energy dispersive spectroscopy (EDS) analysis, which confirmed a composition close to the that of the source target. Atomic force microscopy (AFM) photographs showed an average surface roughness of about 1.0 nm, a value of the same order of that measured in standard Nb films employed in conventional superconducting junction technology.

The low-temperature magnetic properties of as-deposited $Ni_{0.5}Cu_{0.5}$ film have been also investigated. In particular, the magnetization versus temperature of a 100-nm-thick film was measured by using a vibrating sample magnetometer (VSM, Oxford Maglab). Figure 1shows the temperature dependence of the magnetization when a magnetic field of $H=4\times10^5$ A/m is applied. The magnetization curve does not show any saturation at low temperatures as expected in conventional ferromagnetics. Anomalous behaviors have been already observed in NiCu alloy films with a closer composition.[39] A possible explanation can be found in the application of a quite high magnetic field need for the *M* vs *T* measurement. In fact, when a magnetic field *H* is applied, the *M* vs *T* curve has a continuous second derivative, which is negative for $T<T_{Curie}$ and positive for $T>T_{Curie}$. If the magnetic field is quite large and the measurement is carried out down to a T_{min} close to T_{Curie} [in our case $T_{min}=5$ K and $T_{Curie}\approx 20-30$ K as taken by considering the temperature corresponding to 15% of $M(T_{min})$], the change in sign of the second derivative is completely lost and only the positive part is visible. This means that the *M* vs *T* curves of very weak ferromagnetics[40] appear not Curie-Weiss like. Moreover, the estimation of the spontaneous moment per atom $\mu_0=0.06\ \mu_B$/atom at $T=4.2$ K, suggests to exclude the presence of a high degree of spatial inhomogeneity due to the presence of Ni clustering in deposited NiCu film.

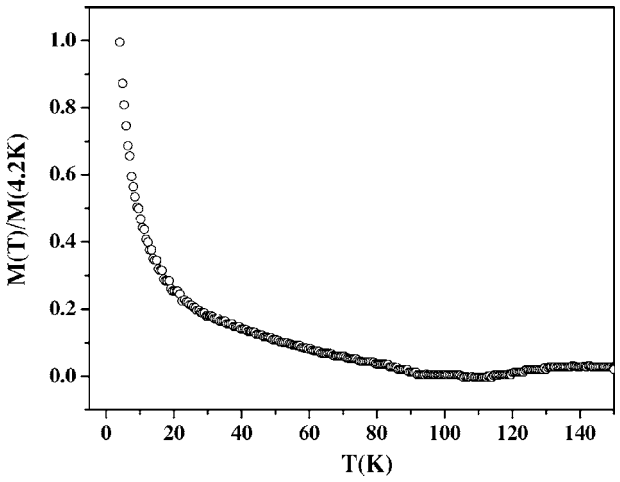

FIG. 1. Magnetization vs temperature of a $Ni_{0.50}Cu_{0.50}$ film of thickness $d_F=100$ nm. An external magnetic field $H=4\times10^5$ A/m was applied.

The resistivity of a thin (20 nm) NiCu film was also measured by using a four-probe in-line technique, and it was found to be $\rho_{NiCi}=0.07$ mΩ cm. The small value of the thickness was chosen according to those used in the fabrication of junction electrodes as discussed in the following.

Superconducting tunnel junctions containing Nb/$Ni_{0.5}Cu_{0.5}$ or $Ni_{0.5}Cu_{0.5}$/Nb bilayers as one of the electrodes were fabricated by using a standard photolithographic process already employed in superconducting electronics technology.[41] In order to avoid any magnetic contamination of the UHV system where the deposition of Nb and Al takes place, $Ni_{0.5}Cu_{0.5}$ films have been sputtered in a different vacuum system. Two configurations have been employed to study the proximity effect on both sides of the S/F bilayer—i.e., Nb/NiCu-I-Nb and NiCu/Nb-I-Nb, where I is the insulating tunnel barrier. We will describe the fabrication procedure concerning just the former configuration, since the description can simply be extended to the latter one. It is important to notice that this fabrication procedure has been adopted because NiCu films were not suitable to be etched

TABLE I. Fabrication parameters.

Sample	A	B	C	D	E
Bottom electrode	Nb (70 nm)	$Ni_{0.50}Cu_{0.50}$ (15 nm)	Nb (70 nm)	Nb (70 nm)	Nb (70 nm)
	$Ni_{0.50}Cu_{0.50}$ (12 nm)	Nb (70 nm)	$Ni_{0.50}Cu_{0.50}$ (25 nm)	$Ni_{0.50}Cu_{0.50}$ (50 nm)	$Ni_{0.50}Cu_{0.50}$ (16 nm)
Tunnel barrier	Al (5 nm)	Al (5 nm)	Al (5 nm)	Al (5 nm)	Al (5 nm)
	Al_xO_y	Al_xO_y	Al_xO_y	Al_xO_y	Al_xO_y
Top electrode	Al (3 nm)	Al (3 nm)	Al (3 nm)	Al (3 nm)	Al (3 nm)
	Nb (250 nm)	Nb (250 nm)	Nb (250 nm)	Nb (250 nm)	Nb (250 nm)

by a reactive ion etching (RIE) process and no anodization oxide was formed on it. After a chemical cleaning of the corning glass substrate, the Nb bottom layer was deposited by magnetron sputtering at a base pressure of 1.0×10^{-7} mTorr by using a lift-off photoresist mask. The sputtering power and the deposition rate were 750 W and 2.2 nm/s, respectively. Without removing the photoresist, the Nb film was introduced in another UHV system, where the surface was preventively cleaned by means of an ion beam etching. The Ar pressure during the etching was 1.5×10^{-4} mbar, while the beam power was 2 W. The etching rate was about 0.2 nm/s, and the etching time was 30 s. Afterward, the NiCu film was deposited and the photoresist mask was removed. By means of a new lift-off procedure, the junction area was defined at the crossing of two perpendicular lines. The base electrode surface was preventively etched by an Ar back sputtering (power 30 W, etching rate 0.03 nm/s) before the deposition of a thin layer of Al by dc magnetron sputtering took place (power 50 W and deposition rate 0.2 nm/s). The low surface roughness of NiCu as evidenced by AFM analyses allowed us to extend the standard technology of Al_xO_y artificial barriers to this case.

The Al surface was thermally oxidized in an O_2 pressure of 40 mbar for 1 h. Finally, a thin layer of Al (3 nm) and the Nb top electrode (250 nm) were deposited in sequence without breaking the vacuum. The former film does not allow a direct contact of the Nb counterelectrode with the oxide layer: this should reduce the oxygen contamination in the near-interface layer of the Nb film. The area of the junctions was $40 \times 40\ \mu m^2$. Table Isummarizes the characteristics of all types of measured junctions.

Samples were measured in a superinsulated LHe Dewar, and were locally shielded by means of a μ-metal box against external electromagnetic fields. The Dewar was pumped by a mechanical pump to reach temperatures down to 1.4 K as read by a Ge thermometer located close to the chip. When necessary, an external magnetic field was supplied by a Cu solenoid able to provide fields up to 1.6×10^3 A/m parallel to the junction plane. The ratios between the static resistance measured at $V=2$ mV—i.e., R_s—and the normal tunneling resistance measured at 6 mV—i.e., R_{nn}—were 3 and 5 at $T=4.2$ K and $T=1.4$ K, respectively.

Current-voltage characteristics (I-V) of the fabricated samples are shown in Fig. 2where they have been vertically shifted for the sake of clarity. By following indications in Table I, the measured Josephson critical current densities were 130 A/cm^2 (sample A), 165 A/cm^2 (sample B), 3 A/cm^2 (sample C), and 6 A/cm^2 (sample E). In sample D no critical Josephson current was measured. The magnetic field pattern of the Josephson critical current as a function of an externally applied magnetic field (I_c vs H) was measured at different temperatures for samples A, B, and C, respectively. All tested junctions exhibit both good modulation of the I_c current and current uniformity. The I_c vs H curve for sample A measured at $T=4.2$ K is shown in Fig. 3. Tested junctions were in the small limit, since the ratio between the junction size L and the estimated Josephson penetration depth λJ was found to be ~ 0.7.

In Fig. 4the normalized conductances dI/dV vs V curves for junctions A and B obtained by numerically differentiating the I-V data at $T=1.4$ K are also shown. The sharpness of such curves demonstrates the BCS-like character of the electronic densities of states of both electrodes. A normalized conductance of a Nb-Al_xO_y-Nb sample is showed in the inset of Fig. 4. A dip after the main peak is also observed. Nevertheless, such a dip is still present in the I-V characteristic of sample B, where the F layer is positioned on the opposite side of the tunnel barrier (see Table I). The occurrence of such a dip has been extensively recognized as due to a not complete oxidation of the Al film during the barrier formation. The study of this structure has a long history, as demonstrated by the large number of both theoretical and experimental papers already published.[41] The origin should be

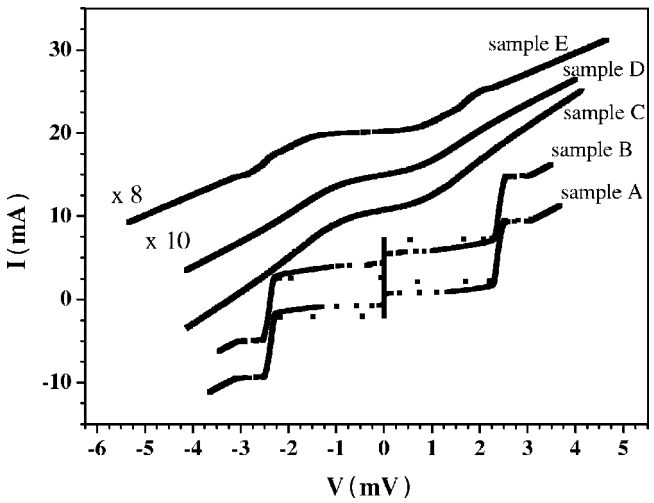

FIG. 2. Current-voltage I-V characteristics for all samples described in Table Iand measured at $T=4.2$ K. Curves have been vertically shifted for clarity.

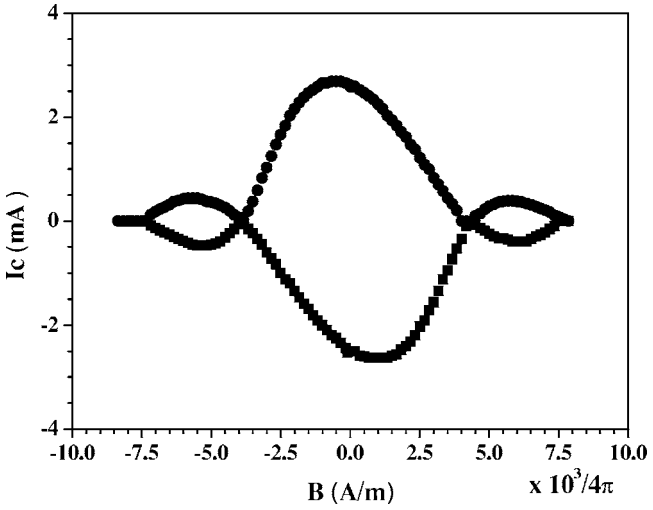

FIG. 3. Josephson critical current vs externally applied magnetic field at $T=4.2$ K for positive (circle) and negative (square) critical current in the case of sample A.

related to the redistribution of the Andreev bound states in a diffusive normal metal in the S/N bilayer. This physical mechanism is not specific for S/N structures, and hence it occurs also in S/F bilayers as well. To describe quantitatively the dip observed in our structures, an extension of the theory is required to the case of a three-layer proximized structure—e.g., S/F/N as realized effectively in our experiments. At present such theory is not available, and it will be the subject of a future study. However, in this paper we are mainly focused in DOS anomalies which are specific signatures of the proximity effect in superconductor/ferromagnet films. We would like just to emphasize that another possible explanation of this negative current region has been recently proposed by Barone and Ovchinnikov,[42] who considered the

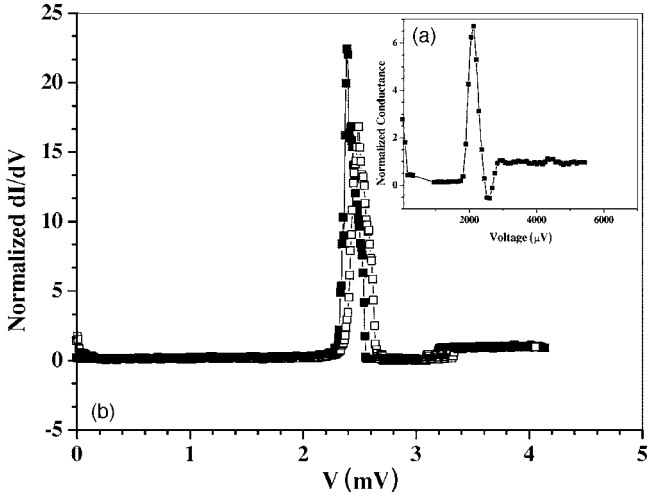

FIG. 4. Numerical conductance vs voltage of samples A (solid square) and B (open square) at $T=1.4$ K after the application of an external magnetic field. In the case of sample B a peak due to a residual Josephson current is also evident. The inset shows the conductance of a basic Nb-Al_xO_y-Nb junction fabricated with the same process.

role of multiparticle tunneling channels in the case of highly transparent tunnel junctions. However, this quite interesting explanation seems to be excluded by the low current densities realized in our samples ($J_c \sim 10^2$ A/cm^2) and the high level of leakage currents, which usually tend to cover these second-order tunnel channels.[43]

III. DISCUSSION

The physical properties of a S/F bilayer can be described by using the microscopic model proposed in Ref. 15, which mainly assumes the dirty limit for the involved materials and an arbitrary finite transparency of the bilayer interface. According to the model, the spatial variation of the superconducting order parameter in F arises as a response of the Cooper pair to the energy difference between the two spin directions, related to the presence of an exchange energy E_{ex} between the two spin populations. The model has been developed in the framework of the general Usadel equations for the S and F layers,[44] whose thickness will be indicated as d_S and d_F, respectively. According to the formalism of Ref. 14, the physical properties of the S/F bilayer are described in terms of two parameters, named γ and γ_B, defined as $\gamma = \rho_S \xi_S / \rho_F \xi_F$ and $\gamma_B = R_B A / \rho_F \xi_F$, where $\rho_{S(F)}$ is the normal state resistivity of the S(F) layer, ξ_S is related to the bulk coherence length in S, and $\xi_F = \sqrt{D_F / 2\pi T_c}$ is the coherence length in the F layer where D_F and T_c are the energy diffusion coefficient and the S layer critical temperature, respectively, and R_B and A are the resistance and the area of the S/F interface. The parameters γ and γ_B have simple physical meanings: γ is a measure of the strength of the proximity effect between S and F layers, whereas γ_B describes the effect of the boundary transparency between them. Under the assumption of dirty limit conditions, the model allows the evaluation of the electronic density of states of the S/F bilayer renormalized to the presence of the exchange field. Figure 5shows some calculated DOS at the F edge of a S/F bilayer in the case $d_S = 1.85\xi_S$, $d_F = 0.7\xi_F$, $E_{ex} = 0.9\pi K_B T_c$, and $T=1.4$ K and for different values of γ [Fig. 5(a)] and γ_B [Fig. 5(b)]. In particular, in Fig. 5(a)the value of γ_B was fixed at $\gamma_B = 0.02$, while in Fig. 5(b)the value of γ was $\gamma = 0.02$, and both of them were chosen close to those considered in the comparison between experimental and theoretical curves as described in the following. The presence of interfaces ensures the presence of scattering centers: as long as the interfaces affect several atomic layers of both films, the boundary conditions are those of the dirty limit as previously discussed. Over a scale length equal to the coherence length in both layers, any solutions for the pair potential and the densities of states are governed by the same equations valid in a dirty superconductor. At depths larger than the coherence length, the fluctuations in pair potential and in densities of states are not relevant, and the behavior tends to that of a bulk superconductor.

By means of a numerical deconvolution technique based on an algorithm proposed by Blamire[45] we extracted the unknown tunneling density of states (TDOS) from the *I-V* characteristics. The main assumption of this numerical code is that the DOS of one of the electrodes is known and sharply

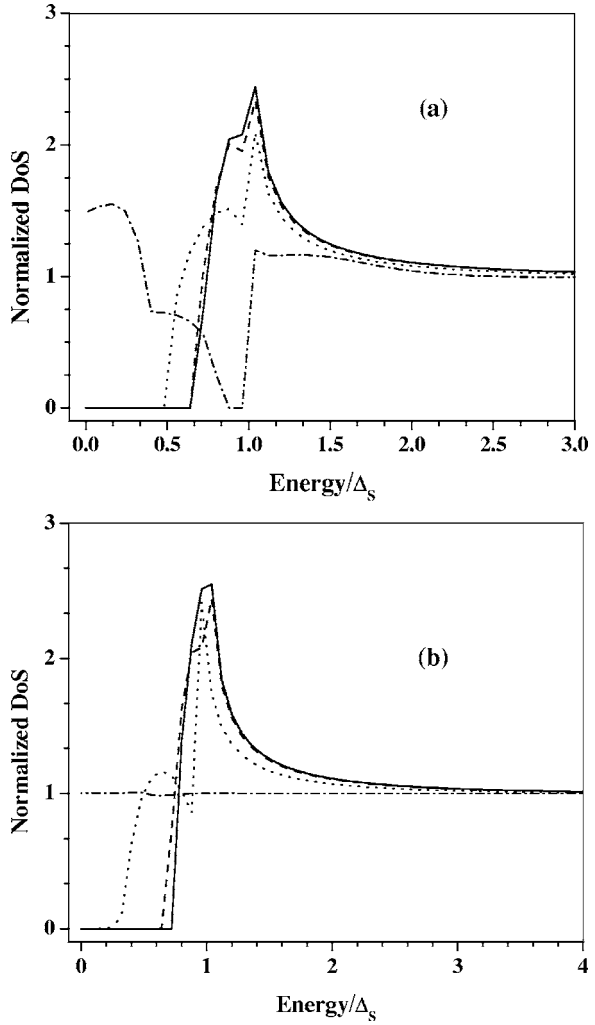

FIG. 5. (a) Normalized DOS vs energy normalized to the energy gap into S at $\gamma=0.02$ and for different values of the γ_B parameter: $\gamma_B=0.002$ (solid line), $\gamma_B=0.02$ (dashed line), $\gamma_B=0.2$ (dotted line), and $\gamma_B=2$ (dash-dotted line). The other parameters are reported into the text. (b) Normalized DOS vs energy normalized to the energy gap into S at $\gamma_B=0.02$ and for different values of the γ parameter: $\gamma=0.002$ (solid line), $\gamma=0.02$ (dashed line), $\gamma_B=0.2$ (dotted line), and $\gamma_B=2$ (dash-dotted line). The other parameters are reported in the text.

peaked at the gap edge in order to minimize the errors during the calculation. Such an assumption is quite justified by the sharpness of the conductance curve as shown in Fig. 4. This method has been successfully used for the evaluation of the TDOS in NbN/Nb and Nb/Al bilayers.[46,47] A BCS-like function for the DOS of the Nb counterelectrode has been assumed with an energy gap $\Delta_S=1.35$ meV. The presence of a high leakage current density ($J_{\text{leak}}=0.14\ \mu\text{A}/\mu\text{m}^2$ at $V=0.5$ mV) in the subgap region represents a limit for the convergence of the deconvolution algorithm. The high leakage current densities are a direct consequence of the employed fabrication procedure, in which the insulation between the two electrodes is realized only by a thermally grown Al oxide covering the bottom layer.

Even if the junctions do not show a very high quality, as reported in literature for standard SNAP or SNEAP fabrication processes,[48] our procedure has the advantage to be more adaptable and easier for structures involving both superconducting and ferromagnetic films. The simplicity of the procedure and the achieved quality are a good compromise in order to effectively combine the Nb tunnel junction technology with the presence of ferromagnetic layers. One of the features evidenced by the *I-V* curves is the overall increase of the quasiparticle current, as demonstrated by the lower resistance in the subgap region. As a consequence, a smaller sum-gap voltage value (V_{sg}) is measured. The problem of leakage currents for $V<V_{sg}$ has been extensively investigated in the past[49] in the framework of tunnel transport in inhomogeneous barriers. Localized electronic states in the barrier add other components into the tunneling current that can be studied in detail by simulating "bad barriers" through the introduction of defects inside the insulating layer. In our samples we believe that the main contribution to subgap leakage currents is due to a not complete insulation along the perimeter of the junction, which introduces spurious low resistances in parallel to that of the junction, increasing the current in the McCumber region.[50] Reproducible *I-V* data concerning standard three-layer deposition junctions[51] show that this anomaly is completely avoided in the case of no vacuum breaking during deposition. Nevertheless, this experimental evidence and the measured smaller critical current do not allow one to exclude an active role of oxygen vacancies belonging to either nanocrystalline Al_2O_3 or Nb_2O_5 in terms of resonant tunneling.[52] The presence of localized states inside the energy barrier can be described by an energy-independent density—i.e., $n_L(E)=$const, to which the leakage current I_L in the $eV<\Delta$ region is proportional. Moreover, a further contribution to I_L will derive from the effective shortening of the tunnel barrier width due to such localized states. We do not believe that such subgap leakages are due to the presence of a ferromagnetic layer nearby the tunnel barrier. In fact, as shown in Fig. 2(see, for example, samples A and B), the *I-V* curves of both configurations have the same features. Nevertheless, the presence of leakage currents produces additional conductance channels in the *I-V* characteristics, which are difficult to model. They contribute in some way to mask and/or smear effects due to the presence of the F film. Also in this case, we focused our attention to the sudden increase of the tunneling DOS and its main peak—i.e., on the region corresponding to energies larger than the energy gap threshold. The deconvolution technique has been applied to *I-V* characteristics measured at the lowest temperatures where the current leakages in the subgap region are minimized.

The comparison between experimental and theoretical DOS curves for samples A and B is shown in Figs. 6(a) and 6(b), respectively. The best agreement was found for γ and γ_B given by $\gamma=0.02$ and $\gamma_B=0.02$, respectively, for device A. In the case of device B the slight change in the F thickness was taken into account. The discrepancy between TDOS and theoretical predictions at $V\sim 1.7$ mV is a consequence of the proximity effect arising from the not fully oxidized Al films in the tunnel barrier formation as previously discussed. According to the adopted deconvolution algorithm, the errors on the tunneling DOS data have been estimated to be of the same order of those affecting current values—i.e., about 5%.

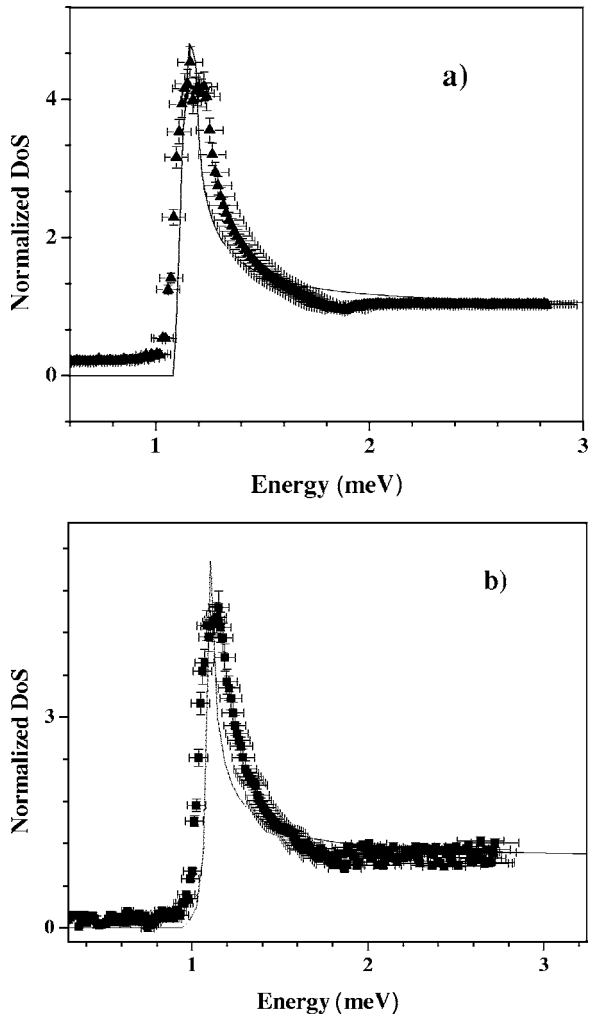

FIG. 6. Comparison between numerical (dashed line) and deconvoluted DOS for sample A (a) and B (b) at $T=1.4$ K.

The numerical deconvolution algorithm has been successfully employed in the comparison of TDOS with various proximity models, and the results in terms of interface transparency and N thickness dependence of the resulting density of states were always very reasonable and consistent with other similar determinations.[47,53] Also in this case the estimations in terms of interface transparency and exchange energy are consistent with the fabrication technology and the weak ferromagnetic nature of the $Ni_{0.50}Cu_{0.50}$ alloy. By taking into account the evaluations for proximity parameters we estimated $\xi_{NiCu} \sim 24$ nm and $E_{ex}=0.9\pi K_B T_{c,Nb} \sim 2.3$ meV at $T=1.4$ K. The value of the coherence length resulted in being slightly larger than that reported in literature for similar weak ferromagnetic layers (see, for example, Ref. 31), and it corresponds to a cleaner S/F interface. Nevertheless, the smaller Ni concentration in the employed films can also justify such a slightly larger value. The results in term of TDOS are clearly less sharp than theoretical ones due to the propagation of noise affecting the *I-V* data, which propagates to the deconvolution curve. The role of noise in the deconvolution technique is anyway extensively discussed in Ref. 45.

By starting from the γ value and assuming a coherence length for the polycrystalline Nb of $\xi_S=10$ nm, we obtained

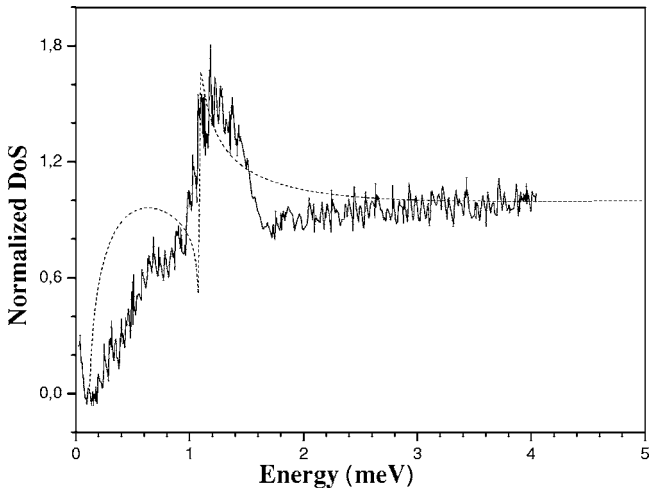

FIG. 7. Comparison between numerical (dashed line) and deconvoluted (solid line) DOS for sample E at $T=1.4$ K.

a value 0.05 for the normal resistivity ratio ρ_{Nb}/ρ_{NiCu} at low temperatures and close to the Nb transition to the superconducting state. According to our previously discussed characterization of NiCu films, the resistivity of the Nb film is of the order of a few $\mu\Omega$ cm at $T=T_{c,Nb}$. This is a quite reasonable result for a polycrystalline Nb with a room-temperature resistivity of the order of tens of $\mu\Omega$ cm and a resistivity ratio $\beta_{10} \leqslant 10$ defined as the ratio between the room-temperature resistivity and that at $T=10$ K—i,e., close to critical temperature of Nb.

Experimental results for sample E in terms of current-voltage *I-V* characteristic and deconvoluted density of states obtained at $T=1.4$ K (see Fig. 7) show a current discontinuity at a voltage $V \sim 0.7$ mV. A current nonlinearity in the *I-V* subgap region of a S_1-I-S_2 superconducting tunnel junction, with S_1 and S_2 the two superconducting junction electrodes, can be ascribed to various physical effects:[54] multiparticle tunneling occurring in high-transparency and low-leakage superconducting tunnel junctions, Josephson resonances, the presence of a two-energy gap material as one of the electrodes, and the energy gap difference between the two electrodes. Apart from this latter hypothesis, excluded by the low operating temperature, all other mechanisms should require high-quality tunnel junctions or exotic hypotheses about the material which are not compatible with the previous junctions characterization. The F nature of one of electrodes could suggest a possible explanation in terms of a spin splitting mechanism,[55] which reflects the two spin distributions splitting due to the presence of an exchange energy. Nevertheless, this explanation at this moment is not completely supported by a high degree of data reproducibility.

The estimation of ξ_F is also qualitatively consistent with experimental results obtained in samples C and D in terms of measured Josephson current. In fact, by assuming for γ, γ_B, and E_{ex}, the previously determined values, and scaling d_F according to different NiCu thickness (see Table I), we numerically calculated the Josephson critical current in such structures according to the theoretical approach proposed in Ref 15in the case of a S/F-I-S superconducting tunnel junction. Numerical calculations predict a strongly reduction of

the Josephson current in the case of sample C ($d_F/\xi_F=1.1$) with respect to sample A—i.e., $J_c(C)/J_c(A)=0.4$ at $T=4.2$ K—and no Josephson current in the case of sample D ($d_F/\xi_F=2.1$). Nevertheless, in our experiments we found $J_c(\text{sample } C)/J_c(\text{sample } A)=0.04$ at $T=4.2$ K, i.e., a ratio which is one order of magnitude smaller than the theoretical value. We ascribed such a discrepancy both to not-well-defined interface parameters occurring in different junctions and a not-complete shielding of the external magnetic field. Further experiments on the Josephson critical current dependence on both temperature and F layer thickness in S/F tunnel devices will be anyway considered in more detail elsewhere.

IV. CONCLUSIONS

In summary, superconducting tunnel junctions containing proximized bilayers formed by a superconductor (Nb) and a weak ferromagnet ($Ni_{0.50}Cu_{0.50}$) have been fabricated and characterized down to $T=1.4$ K in terms of current-voltage I-V curves and Josephson current versus externally applied magnetic field. Moreover, tunneling data have been used to extract the density of states on both sides of such superconductor/ferromagnet (S/F) bilayers by means of a numerical deconvolution algorithm. Results in terms of DOS have been compared with theoretical predictions from a proximity model developed for S/F bilayers in the dirty limit in the framework of Usadel equations. The comparison between tunneling and theoretical density of states allowed us to estimate the main physical parameters characterizing the proximity effect in such Nb/NiCu bilayers. In particular, the resulting values for the coherence length $\xi_{NiCu}\sim 24$ nm and the exchange field energy $E_{ex}=2.3$ meV at $T=1.4$ K are in agreement with those obtained in other experiments.

ACKNOWLEDGMENTS

This work was partially supported by MURST in the framework of the COFIN2001 Program "Technology and applications of cryogenic microdetectors", and NOW-RFBR program 047.016.005 and NanoNed Grant No. TCS.7029. Ya.V.F. was partially supported by the RFBR Grant No. 04_02_16348.

[1] P. G. de Gennes, Rev. Mod. Phys. **36**, 225 (1964).
[2] W. L. McMillan, Phys. Rev. **175**, 537 (1968).
[3] A. V. Zaitsev, Zh. Eksp. Teor. Fiz. **86**, 1742 (1984) [Sov. Phys. JETP **59**, 1015 (1984)]; M. Yu. Kupriyanov and V. F. Lukichev, Sov. Phys. JETP **67**, 1163 (1988).
[4] A. A. Golubov, E. P. Houwman, J. G. Gijsbertsen, V. M. Krasnov, J. Flokstra, H. Rogalla, and M. Yu. Kupriyanov, Phys. Rev. B **51**, 1073 (1995).
[5] J. M. Rowell and W. L. McMillan, Phys. Rev. Lett. **16**, 453 (1966).
[6] E. L. Wolf, *Principles of Electron Tunneling Spectroscopy* (Oxford University Press, New York, 1985).
[7] S. Guéron, H. Pothier, Norman O. Birge, D. Esteve, and M. H. Devoret, Phys. Rev. Lett. **77**, 3025 (1996).
[8] A. A. Golubov and M. Yu. Kupriyanov, J. Low Temp. Phys. **70**, 83 (1988).
[9] W. Belzig, C. Bruder, and G. Schön, Phys. Rev. B **54**, 9443 (1996).
[10] N. E. Booth, in *Superconductive Particle Detectors*, edited by A. Barone (World Scientific, Singapore, 1988).
[11] Z. Radovic *et al.*, Phys. Rev. B **44**, 759 (1991).
[12] A. I. Buzdin, Phys. Rev. B **62**, 11377 (2000).
[13] M. Zareyan, W. Belzig, and Yu. V. Nazarov, Phys. Rev. B **65**, 184505 (2002).
[14] V. N. Krivoruchko and E. A. Koshina, Phys. Rev. B **63**, 224515 (2001); **64**, 172511 (2001); **66**, 014521 (2002).
[15] A. A. Golubov, M. Yu. Kupriyanov, and Ya. V. Fominov, Pis'ma Zh. Eksp. Teor. Fiz. **75**, 223 (2002) [JETP Lett. **75**, 190 (2002)].
[16] F. S. Bergeret, A. F. Volkov, and K. B. Efetov, Phys. Rev. Lett. **86**, 3140 (2001); F. S. Bergeret, A. F. Volkov, and K. B. Efetov, Phys. Rev. B **64**, 134506 (2001); **65**, 134505 (2002).
[17] J. Aarts, J. M. E. Geers, E. Bruck, A. A. Golubov, and R. Coehoorn, Phys. Rev. B **56**, 2779 (1997).
[18] Z. Radovic, M. Ledvij, Lj. Dobrosavljevic-Grujic, A. I. Buzdin, Ya. V. Fominov, N. M. Chtchelkatchev, and A. A. Golubov, Pis'ma Zh. Eksp. Teor. Fiz. **74**, 101 (2001) [JETP Lett. **74**, 96 (2001)].
[19] A. Kadigrobov, R. I. Shekter, and M. Jonson, Europhys. Lett. **54**, 394 (2001); J. Low Temp. Phys. **27**, 760 (2001).
[20] G. Blatter, V. B. Geshkenbein, and L. B. Ioffe, Phys. Rev. B **63**, 174511 (2001).
[21] L. N. Bulaevskii, V. V. Kuzii, and A. A. Sobyanin, Pis'ma Zh. Eksp. Teor. Fiz. **25**, 314 (1977) [JETP Lett. **25**, 290 (1977)].
[22] A. I. Buzdin, L. N. Bulaevskii, and S. V. Panyukov, Pis'ma Zh. Eksp. Teor. Fiz. **35**, 147 (1982) [JETP Lett. **35**, 178 (1982)].
[23] A. I. Buzdin and M. Yu. Kupriyanov, Pis'ma Zh. Eksp. Teor. Fiz. **53**, 308 (1991) [JETP Lett. **53**, 321 (1991)].
[24] E. A. Demler, G. B. Arnold, and M. R. Beasley, Phys. Rev. B **55**, 15174 (1997).
[25] Z. Radovic, L. Dobrosavljevic-Grujic, and V. Vujicic, Phys. Rev. B **63**, 214512 (2001).
[26] S. K. Yip, Phys. Rev. B **62**, R6127 (2000).
[27] T. T. Heikkila, F. K. Wilhelm, and G. Schon, Europhys. Lett. **51**, 434 (2000).
[28] N. M. Chtchelkatchev, W. Belzig, Yu. V. Nazarov, and C. Bruder, Pis'ma Zh. Eksp. Teor. Fiz. **74**, 357 (2001) [JETP Lett. **74**, 323 (2001)].
[29] Yu. S. Barash and I. V. Bobkova, Phys. Rev. B **65**, 144502 (2002).
[30] A. A. Golubov, M. Yu. Kupriyanov, and Ya. V. Fominov, Pis'ma Zh. Eksp. Teor. Fiz. **75**, 709 (2002) [JETP Lett. **75**, 588 (2002)].
[31] V. V. Ryazanov, V. A. Oboznov, A. Yu. Rusanov, V. V. Veretennikov, A. A. Golubov, and J. Aarts, Phys. Rev. Lett. **86**, 2427 (2001).
[32] V. V. Ryazanov, V. A. Oboznov, A. V. Veretennikov, and A. Yu. Rusanov, Phys. Rev. B **65**, 020501 (2002); V. V. Ryazanov, V.

A. Oboznov, A. S. Prokofiev, V. V. Bolginov, and A. K. Feofanov, J. Low Temp. Phys. **136**, 385 (2004).
[33] T. Kontos, M. Aprili, J. Lesueur, and X. Grison, Phys. Rev. Lett. **86**, 304 (2001).
[34] W. Guichard, M. Aprili, O. Bourgeois, T. Kontos, J. Lesueur, and P. Gandit, Phys. Rev. Lett. **90**, 167001 (2003).
[35] Y. Blum, A. Tsukernik, M. Karpovski, and A. Palevski, Phys. Rev. Lett. **89**, 187004 (2002).
[36] T. Kontos, M. Aprili, J. Lesueur, F. Genêt, B. Stephanidis, and R. Boursier, Phys. Rev. Lett. **89**, 137007 (2002).
[37] A. Bauer, J. Bentner, M. Aprili, M. L. Della Rocca, M. Reinwald, W. Wegscheider, and C. Strunk, cond-mat/0312165 (unpublished).
[38] T. Kontos, M. Aprili, J. Lesueur, X. Grison, and L. Dumoulin, Phys. Rev. Lett. **93**, 137001 (2004).
[39] H. Sellier *et al.*, Phys. Rev. B **68**, 054531 (2003); Phys. Rev. Lett. **92**, 257005 (2004).
[40] A. Rusanov, R. Boogaard, M. Hesselberth, H. Sellier, and J. Aarts, Physica C **369**, 300 (2002).
[41] A. A. Golubov, E. P. Houwman, J. G. Gijsbertsen, V. M. Krasnov, J. Flokstra, H. Rogalla, and M. Yu. Kupriyanov, Phys. Rev. B **51**, 1073 (1995); E. L. Wolf, J. Zasadzinski, J. W. Osmun, and G. B. Arnold, J. Low Temp. Phys. **40**, 19 (1980).
[42] A. Barone and Y. Ovchinnikov (private communication).
[43] R. Latempa, Ph.D. thesis, University of Salerno, 2003.
[44] R. Cristiano, L. Frunzio, R. Monaco, C. Nappi, and S. Pagano, Phys. Rev. B **49**, 429 (1994).
[45] K. D. Usadel, Phys. Rev. Lett. **25**, 507 (1970).
[46] M. G. Blamire, Physica C **211**, 467 (1993).
[47] M. G. Blamire, Z. H. Barber, and P. A. Warburton, Physica B **194-196**, 1675 (1994).
[48] M. Gurvitch, M. A. Washington, and H. A. Huggins, Appl. Phys. Lett. **42**, 472 (1983).
[49] J. Halbritter, Surf. Sci. **122**, 80 (1982).
[50] G. Carapella, Ph.D. thesis, University of Salerno, 1999.
[51] H. Kroger, L. N. Smith, and D. W. Jillie, Appl. Phys. Lett. **39**, 280 (1981).
[52] J. Halbritter, J. Appl. Phys. **58**, 1320 (1985), and references therein.
[53] G. P. Pepe, G. Peluso, R. Scaldaferri, A. Barone, L. Parlato, R. Latempa, and A. A. Golubov, Phys. Rev. B **66**, 174509 (2002).
[54] A. Barone and G. Paternó, *Physics and Application of the Josephson Effect* (Wiley, New York, 1982).
[55] X. Hao, J. S. Moodera, and R. Meservey, Phys. Rev. B **42**, 8235 (1990).